Talanta 93 (2012) 186–192

Contents lists available at SciVerse ScienceDirect

Talanta

journal homepage: www.elsevier.com/locate/talanta

LabVIEW control software for scanning micro-beam X-ray fluorescence spectrometer

Pawel Wrobel*, Mateusz Czyzycki, Leszek Furman, Krzysztof Kolasinski, Marek Lankosz, Alina Mrenca, Lucyna Samek, Dariusz Wegrzynek

Faculty of Physics and Applied Computer Science, AGH University of Science and Technology, al. Mickiewicza 30, 30-059 Krakow, Poland

ARTICLE INFO

Article history:
Received 13 October 2011
Received in revised form 31 January 2012
Accepted 6 February 2012
Available online 11 February 2012

Keywords:
X-ray fluorescence (XRF)
Confocal-XRF
LabVIEW programming
Micro-imaging
Spectrometry

ABSTRACT

Confocal micro-beam X-ray fluorescence microscope was constructed. The system was assembled from commercially available components – a low power X-ray tube source, polycapillary X-ray optics and silicon drift detector – controlled by an in-house developed LabVIEW software. A video camera coupled to optical microscope was utilized to display the area excited by X-ray beam. The camera image calibration and scan area definition software were also based entirely on LabVIEW code. Presently, the main area of application of the newly constructed spectrometer is 2-dimensional mapping of element distribution in environmental, biological and geological samples with micrometer spatial resolution. The hardware and the developed software can already handle volumetric 3-D confocal scans. In this work, a front panel graphical user interface as well as communication protocols between hardware components were described. Two applications of the spectrometer, to homogeneity testing of titanium layers and to imaging of various types of grains in air particulate matter collected on membrane filters, were presented.

1. Introduction

Micro-beam X-ray fluorescence spectroscopy (μ-XRF) is a non-destructive technique of elemental analysis widely used in the investigation of metals, environmental and biological samples and for research in archaeology and forensic science. In confocal setup the analysis is performed with primary radiation beam focused by a polycapillary and the secondary radiation emitted by the sample focused by a half-lens polycapillary. The primary beam focusing lens sits in the path between the X-ray source and the sample, whereas the polycapillary half-lens is located between the sample and the detector. The foci of both polycapillaries overlap creating an ellipsoidal testing (probing) volume through which the sample can be translated independently in the 3 spatial dimensions. Typical spatial resolution for a tabletop setup is of the order of few tens of micrometers [1–5].

The purpose of this article is to introduce a tabletop micro-imaging confocal XRF system based on commercially available components. What is new about the present work is that the instrument developed integrates various components which are fully controlled by a LabVIEW program. All programming is performed in the LabVIEW graphical programming language, widely used as a control software development tool [6–10]. Practical advantage of the LabVIEW is that the features typical for real-time systems can be easily achieved, e.g. events handling, process synchronization and code execution parallelization. Almost any hardware component can be controlled using either a dedicated Virtual Instrument (VI) driver or some Windows specific technique (e.g. DDE, DLL). A set of LabVIEW provided software tools can be integrated into VI, allowing realization of a data base, remote program control through Internet, report generation, emergency notification, etc. A front panel of the virtual instrument (graphical user interface) can be designed using controls and indicators from a palette of available elements.

Different virtual instruments (sub-VIs), each executing its own specific function, are wired together on a programming diagram creating a new "VI". The modular feature of LabVIEW allows controlling variety of different hardware modules, and collecting/processing data in parallel.

2. Instrumentation

2.1. System components

A photograph of the experimental setup (configuration without the half-lens) is shown in Fig. 1. The spectrometer consists of: (1) Mo-anode, side window X-ray tube, 50 W, air cooled, 50 μm Mo filter in the primary beam path; (2) silicon drift detector (SDD), active area 10 mm^2, effective thickness 450 μm, 8 μm Be window, FWHM = 140 eV at 5.9 keV; (3) motorized *XYZ* detector stage,

* Corresponding author. Tel.: +48 12 6172956; fax: +48 12 6340010.
E-mail address: Pawel.Wrobel@fis.agh.edu.pl (P. Wrobel).

0039-9140/$ – see front matter © 2012 Elsevier B.V. All rights reserved.
doi:10.1016/j.talanta.2012.02.010

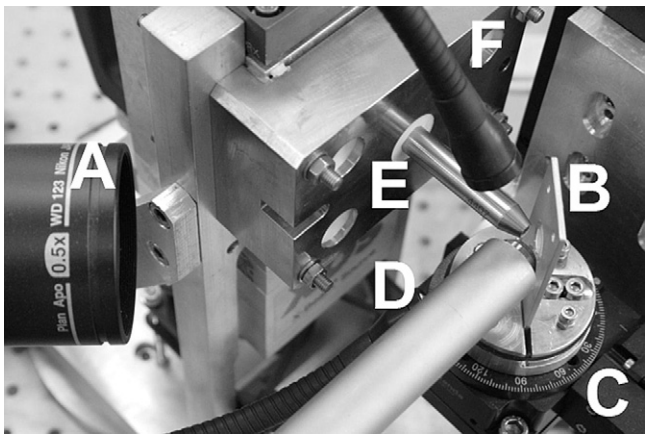

Fig. 1. Photograph of the experimental setup: A – optical microscope lens, B – sample holder, C – *XYZφ* sample stage, D – detector snout, E – X-ray tube with polycapillary, F – light source.

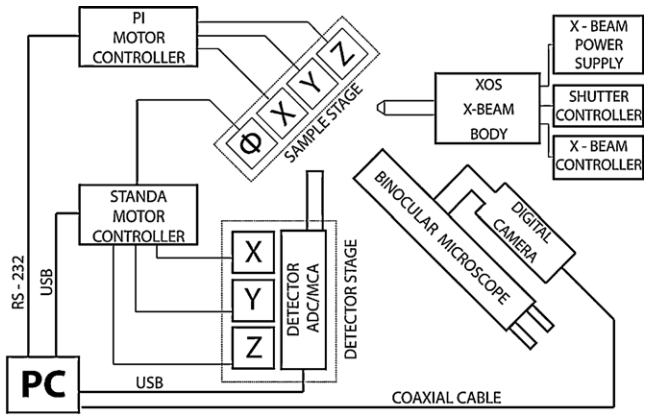

Fig. 2. Schematic diagram of scanning micro-beam X-ray fluorescence spectrometer.

(4) motorized *XYZ*Φ sample stage; (5) optical microscope coupled to a CCD camera; (6) polycapillary X-ray lens, nominal focal distance 4.4 ± 0.3 mm, nominal focal spot diameter, FWHM = 13 μm at Mo-Kα; (7) polycapillary conical collimator (PCCC), nominal focal distance 3.4 mm, nominal focal spot diameter, FWHM = 28 μm at Fe-Kα.

All the system components came with LabVIEW drivers or well-defined software interfaces to be integrated and controlled by the developed virtual instrument (VI). The system was assembled on a stable optical breadboard table from Standa. As a radiation source, the X-Beam from XOS (X-Ray Optical Systems Inc.) which integrated X-ray tube (Mo anode) and optic is utilized. The tube operates with air cooling and is powered by a maximum current of 1 mA at a maximum voltage of 50 kV. The second component of X-Beam is an integrated high voltage power supply and stability controller designed to provide stable X-ray output over the full 50 W operating range. The X-Beam source contains a shutter for switching on and off the X-ray output of the tube.

A silicon drift, Peltier cooled X-ray detector, AXAS-V from Ketek, with resolution of 144 eV at 5.9 keV is positioned perpendicularly to the photon beam (on the horizontal plane). The AXAS-V detector comprises the following components: preamplifier, shaping amplifier, temperature control, internal power supply, ADC/MCA (analog to digital converter/multichannel analyzer) with USB PC interface. The accompanying software, running under MS Windows operating system, provides full control of the ADC/MCA to initiate the measurements and to transfer data. It facilitates a DDE (Dynamic Data Exchange) server and uses the DDE standard protocols to communicate with other Windows programs, such as a LabVIEW client of the DDE server.

X-ray detector together with the AXAS signal processing electronics are mounted on a stack of three (*XYZ*) translational stages 8MT167-25 (Standa) driven by stepper motors. The nominal spatial resolution of this device is 0.156 μm and travel range 25 mm. The (*XYZ*) stages are controlled by PC via USB interface with software access through NI VISA driver. The 8SMC1-USB motor controller came with a suite of software tools (VI's) for controlling the motors and software development using the NI LabVIEW.

The sample table translation axes (*XYZ*) are driven by the Physik Instrumente (PI) M-405CG stages with a travel range of 50 mm. All stages are equipped with high resolution DC motors and gear head drive providing 0.1 μm minimum incremental motion (unidirectional repeatability 0.2 μm). They are controlled by a C-848 PI motor controller. Additionally, a motorized rotation stage 8MR-151 from Standa is employed.

The C-848 and the sample stages are controlled from a host computer via an RS-232 serial connection with ASCII commands that are used to set operating modes, to transfer motion parameters, and to query the system and motion values. A collection of LabVIEW VI's is used to communicate with the C-848 and its connected axes.

A video camera (Bosh LTC0455) coupled to optical microscope focused on the sample is utilized to display details of the area excited by X-ray beam. It is connected to a frame grabber ad-in card (NI-1411) installed in PC running MS Windows XP operating system. Camera control development was carried out in LabVIEW, using NI Vision Acquisition Software with NI-IMAQ camera driver. A scheme of the experimental setup is shown in Fig. 2.

2.2. The program

2.2.1. Front panel

The main software (further called the Main VI) allows user to control all spectrometer parameters automatically. It handles several different modes of measurements. At first the Main VI gives the possibility of precise sample positioning – spectra can be collected in any point. Secondly user can set up and start one-, two- or three-dimensional scanning of the sample. In such a measurement the Main VI moves the sample to the desired points and collects spectra automatically. Additionally several scanning areas can be defined in a "batch file". The Main VI graphical user interface (GUI) was shown in Fig. 3. Most important input/outputs are:

"Probe move" tab – this tab contains menu for controlling the sample translations in 3 spatial directions.
"Autoscan" tab – In this menu user can set up automatic one-, two- or three-dimensional scans, batch file with programmed scanning areas can be also opened here.
ROI (region of interest) tabs – three different regions of interest can be selected from X-ray fluorescence spectrum, the maps of ROI intensities versus the sample position are built and simultaneously displayed during the scan. Number of ROIs which can be displayed during the measurement is limited to simplify block diagram of the software. Other ROIs can be processed offline. During the three dimensional measurement only one single slice is shown.

The Main VI GUI gives also the possibility to choose the live time of measurement and the format of the file in which the X-ray spectra are stored. An additional program called the Camera VI can also be opened here.

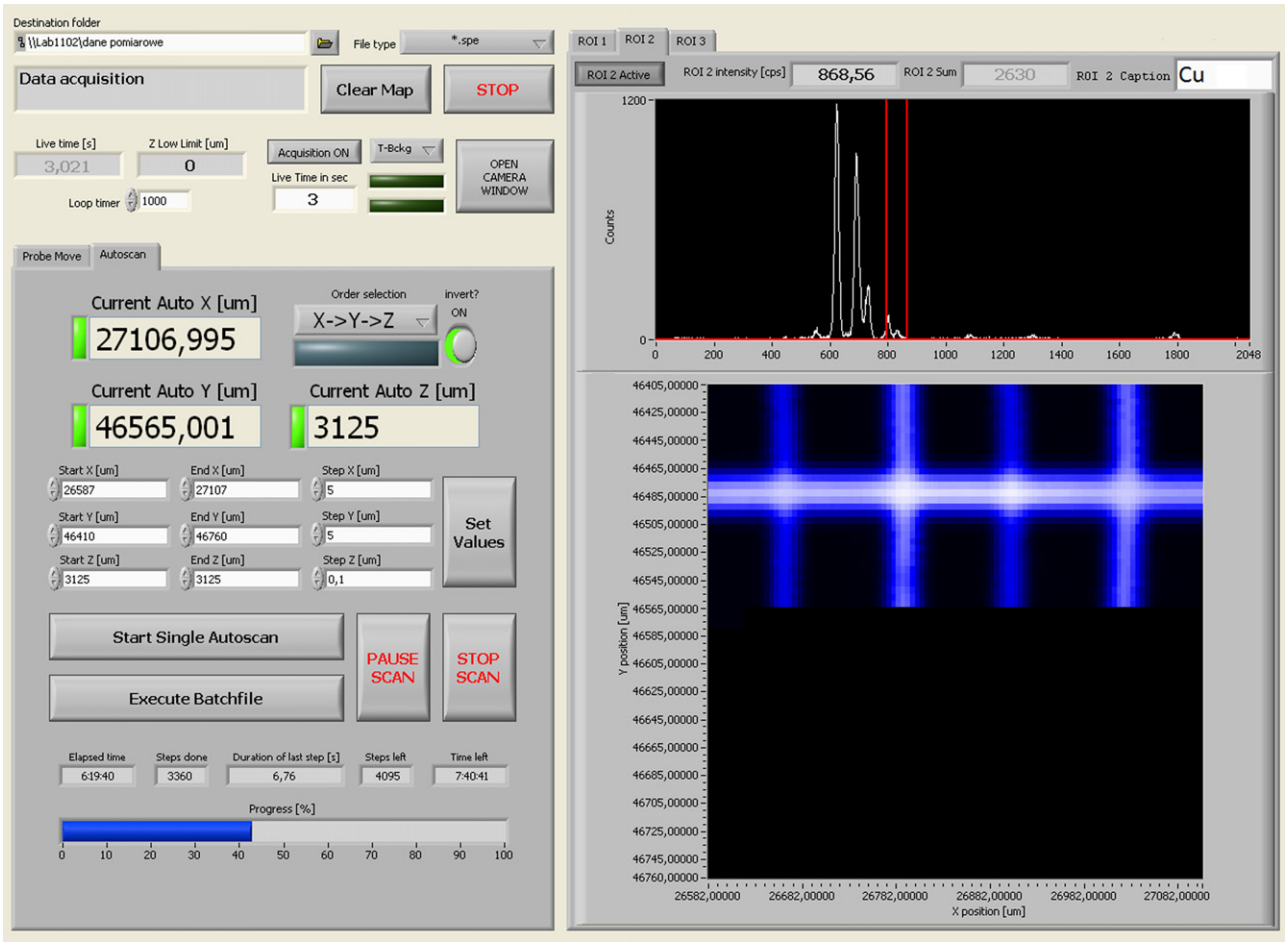

Fig. 3. Screenshot of the front panel of the main VI. Detailed description in the text.

2.2.2. Communication with hardware

Communication with Ketek detector and its integrated ADC is achieved via DDE server. MCA Server and MCDWIN (Ketek's acquisition software) are started together with the Main VI. During the initialization the "live-time preset" is enabled and set. "Range" of data (number of ADC channels) is also requested by the server.

X-ray spectrum can be collected as soon as the initialization is finished. DDE server does not indicate the end of spectrum collection (the only requests are "data" and "data range") so the VI has to find this very moment in order to avoid time or data loss. The VI waits until the total sum of counts in the spectrum (full range integration) stops changing. This procedure is shown in Fig. 4.

MCDWIN delivered actual live-time can be a bit larger than live-time preset (the excess ranges from 0 to 400 ms). This phenomenon is especially significant during short measurements, so it is crucial to get exact information about the actual value of the live-time. Fortunately, the accurate live-time is stored in MCDWIN spectra ASCII file. For each measurement point this information is read from the stored spectrum. The spectrum acquisition procedure produces additional dead time in the range from 1.5 s to 2 s per spectrum acquisition.

Communication with PI controller was realized through dedicated sub-VI's delivered with the entire PI stage system. These sub-VI's are responsible for communication between the Main VI and PI C-848 motor controller. The most important sub-VI's are: MOV.vi – responsible for sending destination position to the controller and starting the axis motion, and POS?.vi providing information about present position of stages.

To avoid any differences between the hardware and software positions of stages an initialization procedure has been created. This procedure moves all axes to a reference position (in the middle of their range of movement) or so called limit position (detected by built-in sensor of M-405CG motor). It is done with the help of a dedicated VI that precedes the Main VI operation. Time loss created during stage movement depends on applied step. For steps smaller than 50 μm it does not exceed 250 ms. Current positions of all axes are stored in a file to avoid multiple initializations before every start of the Main VI. These positions are also being saved during the Main VI operation.

2.2.3. Camera VI

The front panel of the video camera VI is shown in Fig. 5. Main input/outputs are current camera image display and sample stage control panel. This program allows to move the sample perpendicularly to the microscope axis and to select areas for μ-XRF measurements. Camera image display gives information about real-world coordinates of the sample position – current cursor position is real-time recalculated to X-Y motor real-world position. This is done after calibrating the camera – scale has to be calculated for each microscope magnification. The scale computing algorithm is shown in Fig. 6. This routine uses characteristic points or patterns in the image of a translated sample combined with known distance traveled by a motor (12 translations are used) to calculate the *xy* scale calibration factors (in millimeter per pixel).

The X-ray beam position is marked in the camera live-image – it is achieved with the use of fluorescent screen. In the image of the sample an area for scanning (image ROI) is selected. Image ROI can

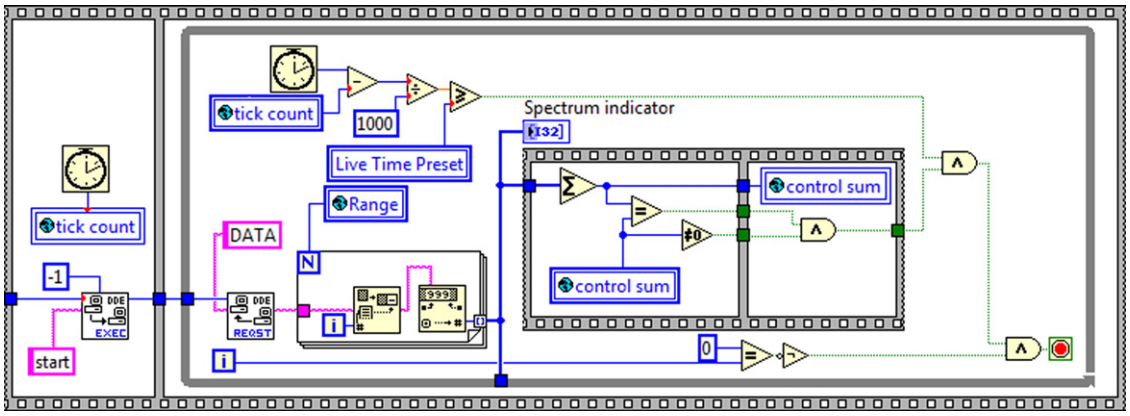

Fig. 4. Spectrum acquisition loop. If the preset live time elapse and total sum of spectra (control sum) does not change the loop stops.

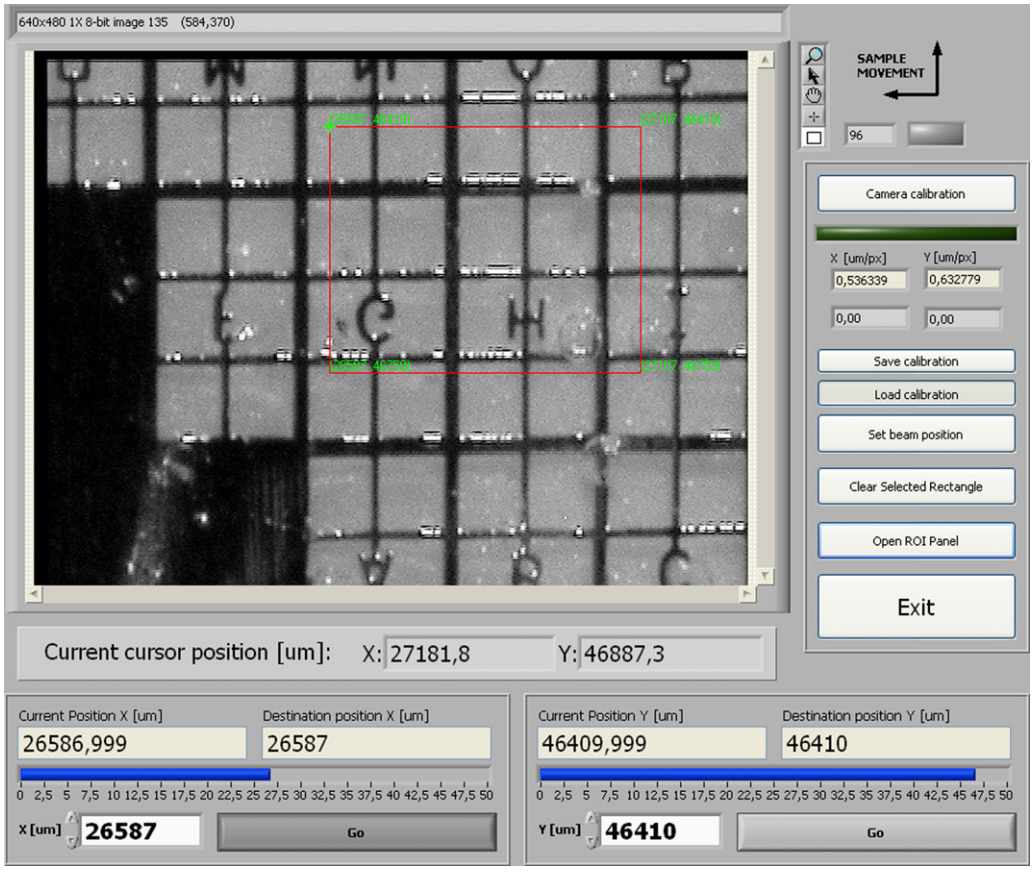

Fig. 5. Screenshot of the front panel of the camera VI. Sample stage control panel is located on the bottom of the front panel.

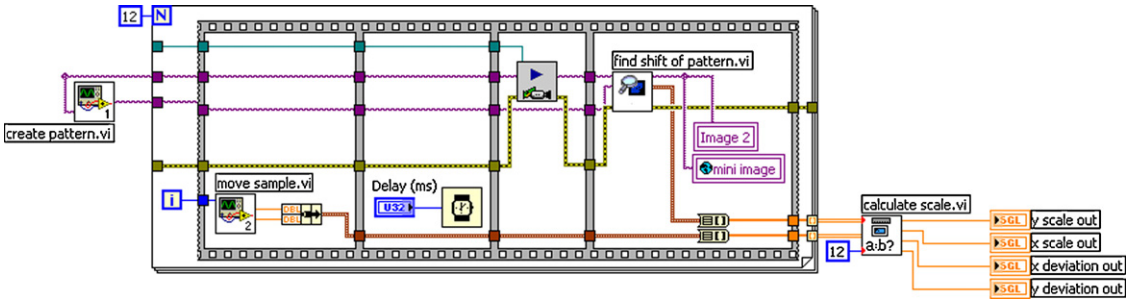

Fig. 6. Scale computing algorithm. Translation of the sample and finding the shift of chosen pattern are repeated 12 times.

also be stored in a file (several different image ROIs can be stored). In Figs. 3 and 5 the screenshots of the Main (Fig. 3) and Camera (Fig. 5) VIs, taken during the measurement, are shown. In Fig. 5 the selection of the area for measurements (here a copper calibration mesh acted as a sample) via the microscope is shown and in Fig. 3 the ongoing measurement controlled with the Main VI is shown.

For communication between PC and the camera – the *Vision and Motion* package together with camera software from NI were used. The calibration algorithm utilizes pattern matching function *FindPatternPosition* and *getScale* from the *Vision and Motion* package. There is no possibility to operate Camera VI and Main VI simultaneously. Actual position of all motors is stored in the file during the operation of both VIs.

2.2.4. Data storage and processing

All collected spectra are saved in *.spe (GAANAS) file format or/and *.xls file. All other data (positions, ROI integrals, exact live-time) are stored in a "scanfile". For every scan a dedicated data folder is created. This folder contains: a subfolder with *.spe files, subfolder with *.xls files and a "scanfile". After each measurement it is also possible to send the data via e-mail.

All spectra are processed by a well-known software package QXAS. The *.spe files are fitted utilizing AXIL, which is included in the QXAS. After each measurement the Main VI creates a batchfile for AXIL which enables the user to fit large number of X-ray spectra automatically with user-defined model. The outcomes of AXIL are net peak areas (with their uncertainties) for all the selected elements and their X-ray peaks. These data (stored in *.asr files) are subsequently normalized to the live-time and appended to the "scanfile" (by another dedicated VI). The result of this operation is a spreadsheet file containing all the data collected during a scan: *XYZ* positions, live-times and net peak areas for all element lines and for all measurement points. Such a file can be used as input for further calculations.

3. Results and discussion

3.1. Characterization of the setup

Size of primary X-ray beam was investigated by using wire scan method [11]. Tungsten wire of 3 μm diameter was used. Vertical and horizontal size of the beam was measured to check the symmetry. The size of the focal spot of the capillary full lens was 16.6 μm vertically and 16.2 μm horizontally.

Minimum detection limits were determined by measuring several certified thin film samples of different elements (pure elements: Ti, Cr, Fe, Cu, Se, Au, Pb and compounds: KI, ZnTe, TbF_3, SrF_2) For each standard sample 25 measurements at different points were done (50 s per point, 50 kV operating voltage, 1 mA tube current). The cumulative spectrum of all points was used to calculate minimum detection limits with the following formula:

$$\mathrm{MDL} = \frac{3\sqrt{N_B}}{N_P} m_S \tag{2}$$

where N_B is the background area, N_P is the net peak area and m_S is a surface mass of element. Calculated minimum detection limits are presented in Table 1.

Table 1
Minimum detection limits for measured elements.

Element	Line	MDL [ng/cm^2]
K	Kα	23.10
Ti	Kα	26.43
Cr	Kα	20.62
Fe	Kα	15.19
Cu	Kα	25.33
Zn	Kα	16.04
Se	Kα	39.25
Sr	Kα	34.97
Te	Lα	71.00
Tb	Lα	33.85
Au	Lα	62.53
Pb	Lα	68.52

3.2. Homogeneity testing of Ti layers

Investigation of the homogeneity of titanium coating on a polymer substrate was performed. Two samples with different titanium coating thickness were examined. The aim of this measurement was to find the mean surface mass of titanium, M_{Ti}, and its relative uncertainty due to the layer intrinsic heterogeneity. Both samples were measured at several thousand points (with 50 μm step). The X-ray tube was operated at 50 kV/1 mA. Time of measurement was 5 s per point for the "thick" sample and 60 s for the "thin" sample. For each sample, the observed relative variance of the sample surface mass was determined from the set of n measured points:

$$s^2_{\mathrm{observed}} = \frac{1}{(M_{Ti})^2} \frac{\sum_{i=1}^{n} (M_{Ti,i} - M_{Ti})^2}{n-1} \tag{3a}$$

$$M_{Ti} = \frac{\sum_{i=1}^{n} M_{Ti,i}}{n} \tag{3b}$$

There were two main contributions to the observed variance: (1) the measurement methodology – s^2_{method} and (2) the sample intrinsic homogeneity – s^2_{homog} [12]:

$$s^2_{\mathrm{observed}} = s^2_{\mathrm{method}} + s^2_{\mathrm{homog}} \tag{4}$$

For the "thin" sample the surface masses at different points, $M_{Ti,i}$, were calculated by adapting a thin sample model in which the intensity of fluorescence radiation (I) is proportional to the surface mass of titanium (M_{Ti}):

$$I = \int_{E_{Ti}}^{E_{\max}} K_{Ti}(E)\mathrm{d}I_0(E)M_P = K'_{Ti}M_{Ti} \tag{5}$$

$K_{Ti}(E)$ is a product of Ti-Kα peak production cross-sections including detection efficiency, $\mathrm{d}I_0(E)$ is a relative number of primary photons with energy E, E_{Ti} is the energy of the titanium photoelectric absorption K-edge, and $E_{\max}$ is the maximum energy of the primary photons. For the "thick" sample "intermediate thickness" sample model was adapted by using effective excitation energy E_{eff} = 17.4 keV:

$$I = \int_{E_{Ti}}^{E_{\max}} K_{Ti}(E)\mathrm{d}I_0(E)M_{Ti}\frac{1-\exp\left\{-M_{Ti}b(E)\right\}}{M_{Ti}b(E)}$$

$$\approx K'_{Ti}\frac{1-\exp\left\{M_{Ti}b(E)\right\}}{M_{Ti}b(E)} \tag{6a}$$

$$b(E_{\mathrm{eff}}) = \frac{\mu_{Ti}(E_{\mathrm{eff}})}{\sin\varphi} + \frac{\mu_{Ti}(E_{Ti-K\alpha})}{\sin\psi} \tag{6b}$$

Table 2
Results of homogeneity testing of Ti layers.

Sample	Number of points	Mean surface mass, M_{Ti} [μg/cm^2]	s_{observed} [%]	s_{method} [%]	s_{homog} [%]
1 (thin)	1491	4.63	5.78	3.18	4.83
2 (thick)	2555	2519	9.42	0.48	9.41

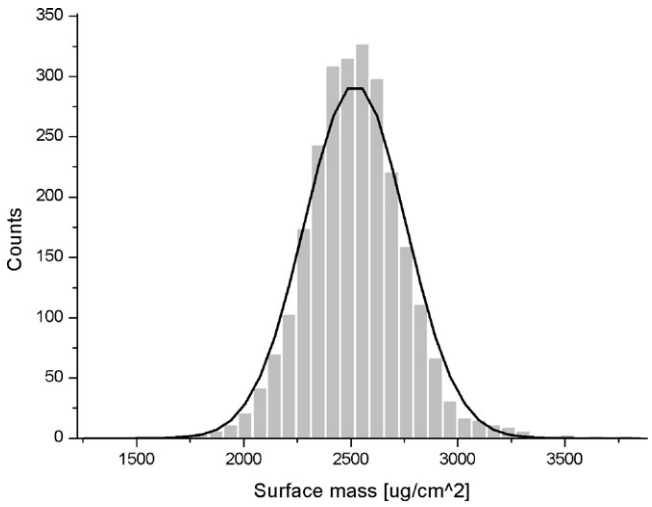

Fig. 7. Surface mass histogram for "thick" sample.

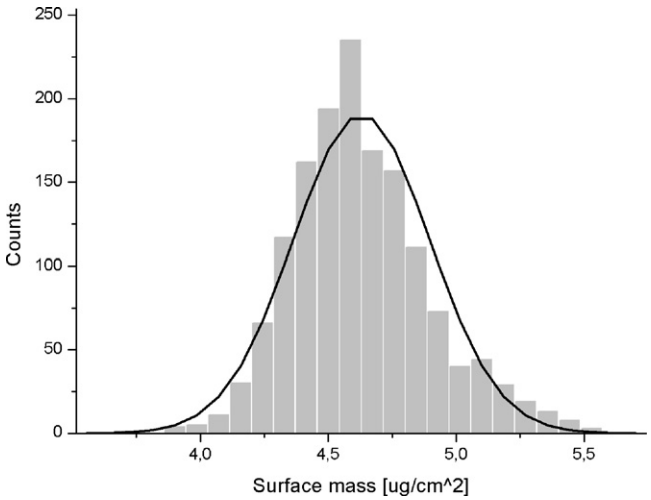

Fig. 8. Surface mass histogram for "thin" sample.

where φ, ψ are the incidence and exit angles, respectively, and $\mu_{\mathrm{Ti}}(E_{\mathrm{eff}})$ and $\mu_{\mathrm{Ti}}(E_{\mathrm{Ti\text{-}K\alpha}})$ are the titanium mass absorption coefficients for effective excitation energy and for the average energy of Ti-Kα peak, respectively. For the "thin" sample, the surface mass of titanium at the i-th position was determined based on Eq. (5):

$$M_{\mathrm{Ti},i} = \frac{I_i}{K'_{\mathrm{Ti}}} \tag{7}$$

and for the "thick" sample based on Eqs. (6a) and (6b):

$$M_{\mathrm{Ti},i} = -\frac{1}{b(E_{\mathrm{eff}})} \ln\left\{1 - I_i \frac{b(E_{\mathrm{eff}})}{K'_{\mathrm{Ti}}}\right\} \tag{8}$$

The sensitivity factor K'_{Ti} was calculated by measurement of thin titanium standard sample with known surface mass (41.6 μg/cm^2).

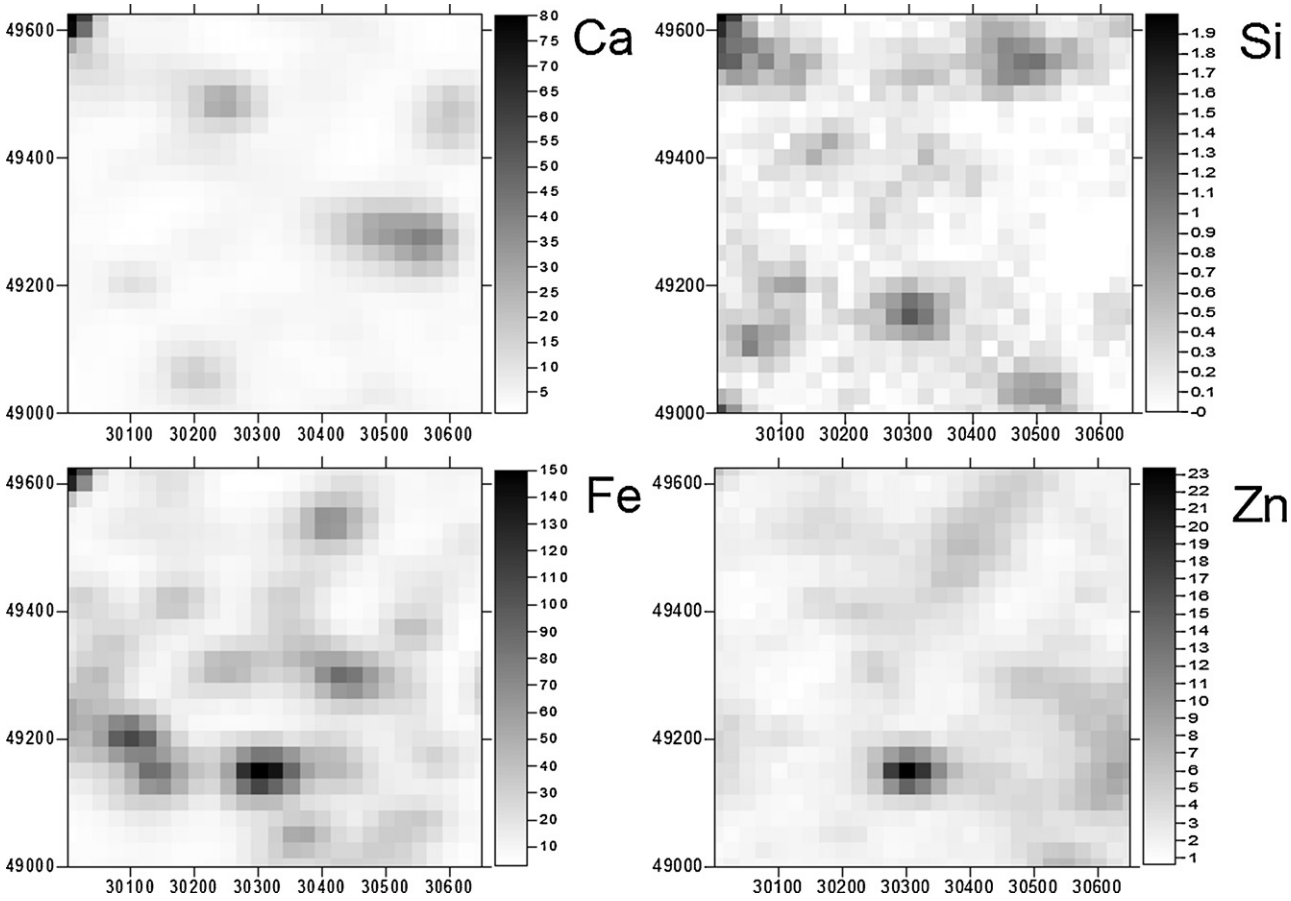

Fig. 9–12. Intensity maps of Ca-Kα, Si-Kα, Fe-Kα and Zn-Kα on the surface of filter. All grey level scale bar values in counts per second (cps). The x- and y-axes scaled in micrometers.

This sample was measured in 25 points with 50 s live time per point. For each point, individual value of $K'_{\mathrm{Ti},i}$ was calculated:

$$K'_{\mathrm{Ti},i} = \frac{I_{\mathrm{std},i}}{M_{\mathrm{Ti,std}}} \tag{9}$$

where $I_{\mathrm{std},i}$ is the intensity of Ti-Kα peak at i-th point and $M_{\mathrm{Ti,std}}$ is the certified surface mass of Ti in the standard sample. The X-ray tube current and voltage were kept the same as for the unknown Ti samples. The set of 25 measurements was used to calculate the average value of K'_{Ti}:

$$K'_{\mathrm{Ti}} = \frac{\sum_{i=1}^{n} K'_{\mathrm{Ti},i}}{n} \tag{10}$$

For fixed values of the parameters K'_{Ti} and $b(E_{\mathrm{eff}})$ the method variance arises due to the propagation of the counting statistic fluctuations through Eqs. (7)–(8). To estimate the expected value the method variance the law of uncertainty propagation was used assuming Poisson distribution of the counting statistics. The expected relative variance of method for the "thin" sample was calculated as

$$s^2_{\mathrm{method}} = \frac{1}{K'_{\mathrm{Ti}} M_{\mathrm{Ti}} t}\left(1 + \frac{2B}{K'_{\mathrm{Ti}} M_{\mathrm{Ti}} t}\right) \tag{11}$$

where t and B denote the measuring time per point and the average number of counts in the background under the Ti-Kα peak, respectively. The relative uncertainty of the layer surface mass due to its inhomogeneity was calculated by rearranging Eq. (5):

$$s_{\mathrm{homog}} = \sqrt{s^2_{\mathrm{observed}} - s^2_{\mathrm{method}}} \tag{12}$$

The results of the measurements are presented in Table 2, additionally histograms of surface masses (with calculated Gauss shape) for both samples are shown (Figs. 7 and 8).

3.3. Two-dimensional imaging of air particulate matter collected on thin filter

Measurement of particulate matter collected on thin polycarbonate filter (NUCLEPORE) was done. The coarse fraction of the particle size (>8 μm) was chosen due to possibility of measurement of single particles. The area of 625 μm × 650 μm with 25 μm step (which gives 702 measurement points) was scanned. Time of measurement was 250 s per point, X-ray tube voltage and current were, respectively, 50 kV and 1 mA. Measured distributions of Kα peak intensities of Si, Ca, Fe and Zn are shown in Figs. 9–12. As one can notice there are certain regions where the intensities are quite high indicating the presence of a particle or a few particles abundant in that element. One can also notice the correlation of signals of Fe and Zn. These elements usually have anthropogenic origin. For particles with the diameters significantly smaller that the primary beam FWHM (about 20 μm) it is not possible to distinguish if the signal originated from a single particle or a conglomerate of several particles. Nevertheless one can still detect presence of different types of particles in the filter. Using spatial and intensity information it is possible to discriminate the major particle types and their eventual correlations, which should lead to identification and apportionment of particle sources. Contrary to the source apportionment methods based on bulk analysis[13,14], which require a number of filters collected at different periods of time characterized by variable contributions from investigated sources, such analysis could be performed based on mapping just a single filter containing sufficient number of particles from specific sources.

4. Conclusions

The goal of this work was to create user-friendly integrated control software for X-ray fluorescence measurements. Its reliability was confirmed by preliminary measurements. As a next step three-dimensional measurements in confocal geometry will be performed. It was confirmed that LabVIEW graphical programming gives a great possibility for controlling large number of different hardware devices. It also simplifies development and further modification of a hybrid system. Any hardware with LabVIEW drivers, or well-defined software interfaces can be incorporated into the LabVIEW program. Sub-VIs representing new hardware functionalities can be directly placed and wired in the program's diagram. In the future the μ-XRF spectrometer will be upgraded with additional detector and distance sensor for precisely measuring the sample position. XOS X-Beam system will be also upgraded with A/D and D/A converters to allow computer control of X-ray beam parameters (current and voltage) and shutter.

Acknowledgement

The authors acknowledge the support by the Polish Ministry of Science and Higher Education and its grants for Scientific Research.

References

[1] B. Kanngiesser, W. Malzer, A.F. Rodriguez, I. Reiche, Spectrochimica Acta Part B 60 (2005) 41–47.
[2] K. Tsuji, K. Nakano, X-Ray Spectrometry 36 (2007) 145–149.
[3] X. Lin, Z. Wang, T. Sun, Q. Pan, X. Ding, Nuclear Instruments and Methods in Physics Research B 266 (2008) 2638–2642.
[4] K. Nakano, K. Tsuji, Journal of Analytical Atomic Spectrometry 25 (2010) 562–569.
[5] I. Mantouvalou, K. Lange, T. Wolff, D. Grotzsch, L. Luhl, M. Haschke, O. Hahn, B. Kanngiesser, Journal of Analytical Atomic Spectrometry 25 (2010) 554–561.
[6] C. Wagner, S. Armenta, B. Lendl, Talanta 80 (2010) 1081–1087.
[7] W. Xu, F.D. McDaniel, Nuclear Instruments and Methods in Physics Research B 241 (2005) 890–895.
[8] G.C.-Y. Chan, G.M. Hieftje, Spectrochimica Acta Part B 60 (2005) 1486–1501.
[9] N.R.J. Poolton, B.M. Towlson, B. Hamilton, D.A. Evans, Nuclear Instruments and Methods in Physics Research B 246 (2006) 445–451.
[10] P. Hosek, T. Prykari, E. Alarousu, R. Myllyla, Journal of the Association for Laboratory Automation 14 (2009) 59–68.
[11] D. Wegrzynek, R. Mroczka, A. Markowicz, E. Chinea-Cano, S. Bamford, X-Ray Spectrometry 37 (2008) 635–641.
[12] L. Kempenaers, L. Vincze, K. Janssens, Spectrochimica Acta Part B 55 (2000) 651–669.
[13] L. Samek, Microchemical Journal 92 (2009) 140–144.
[14] J. Vercauteren, C. Matheeussen, E. Wauters, E. Roekens, R. van Grieken, A. Krata, Y. Makarovska, W. Maenhaut, X.G. Chi, B. Geypens, Atmospheric Environment 45 (2011) 108–116.